Adiabatic Interaction Leading to the Avoided Crossing between the Twin $3^1\Delta_g$ and $4^1\Delta_g$ Rydberg States in Na_2

Thou-Jen Whang,[†] Chanchal Chaudhuri,[‡] Ray-Yuan Chang,[‡] Wei-Xiang Chen,[‡] and Chin-Chun Tsai*[,‡]

Department of Chemistry, National Cheng Kung University, Tainan 70101, Taiwan, and Department of Physics, National Cheng Kung University, Tainan 70101, Taiwan

Received: June 21, 2008; Revised Manuscript Received: March 6, 2009

We present detailed investigations of our previously reported observations of the $3^1\Delta_g$ and $4^1\Delta_g$ Rydberg states having separated-atom limits of Na(3s) + Na(4d) and Na(3s) + Na(4f), respectively, of Na_2 using high-resolution cw optical−optical double resonance spectroscopic measurements and analyzing the assigned rovibrational energy levels both by the individual linear fit method and the Dunham polynomial fit method. We have sorted out e/f-parity observed energy levels, and then from the Dunham polynomial fits of the e-parity levels, we have derived molecular constants and constructed Rydberg−Klein−Rees potentials of the $3^1\Delta_g$ and $4^1\Delta_g$ states, which appear to be twin states with an avoided crossing at $R_c = 4.10$ Å and a splitting of $\Delta E_c = 94$ cm^{-1}. The potentials are in good agreement with the ab initio calculations and linear fit results. The Λ-doubling splittings and the (f−d) *l*-mixing are investigated. A detailed discussion is focused on the adiabatic interaction of the perturbed molecular wave functions/states causing mutual amplitude/intensity sharing giving rise to avoided crossing between the $3^1\Delta_g$ and $4^1\Delta_g$ states.

1. Introduction

Alkali dimers have hydrogen-like *n*s-electronic structure of the outermost shell and transitions in the visible range. They have been extensively investigated both experimentally and theoretically. They have played an important role in understanding the interactions and other fundamental physical properties in diatomics. A lot of attention was paid in investigating Na_2 using high-level ab initio calculations[1,2] and experimental techniques which brought to us many interesting and unusual features such as long-range hyperfine interactions,[3] avoided crossing shelves,[4,5] double minima,[6] pure long-range states,[7] and quantum tunnelling of a potential barrier,[8] illustrating the existence of different types of interactions.

Nowadays, high monochromaticity of the laser coupled with better electronic devices has made it possible to observe the rovibrational state-to-state selective transitions and enables us to identify previously unobserved electronic states. On the basis of the dominant hydrogenic $nl\lambda$ characters of the Rydberg orbital as core-penetrating versus core-nonpenetrating states, a relabeling and classification of the Rydberg states have been reported by J. Li et al.[9] This classification suggests that if the Rydberg states of Na_2 are experimentally observed with two-step excitation via the intermediate $A^1\Sigma_u^+$ ($p\sigma$) and $B^1\Pi_u$ ($p\pi$) states, it is most likely that only low-*l* (<3) penetrating states can be observed due to the $\Delta l = \pm 1$ rule. For instance, core-penetrating ($d\delta$) states, the $1^1\Delta_g$,[10] $3^1\Delta_g$,[11] $5^1\Delta_g$,[12] and $n^1\Delta_g$ ($n = 6-11$)[11] states, have been observed. In addition, one core-nonpenetrating state $2^1\Delta_g$[13] has also been observed.

A brief summary of results of the observations of the $3^1\Delta_g$ and $4^1\Delta_g$ states clumped together like twin potential curves in Na_2 can be found in ref 14. As seen in Figure 1 of ref 14, the congested potential curves above 35 000 cm^{-1}, which dissociate to 3p + 3p, 3s + 4d, and 3s + 4f of Na_2 from ab initio calculations by Magnier,[2] cause difficulties for observation. In particular, ab initio calculations[1] show very close minima (a separation of 120 cm^{-1}) and an avoided crossing point around 4 Å between the penetrating $3^1\Delta_g$ (3s + 4d) state and nonpenetrating $4^1\Delta_g$ (3s + 4f) state. There is also an avoided crossing point around 8 Å between the $2^1\Delta_g$ and $3^1\Delta_g$ states. Therefore, the molecular wave functions near potential minima of these states involve mixed properties of 4p, 4d, and 4f atomic wave functions. Carlson et al.[11] have reported two consecutive bands at this energy region, but it was hard to see any further interactions from their preliminary results. Further, because of the avoided crossing and atomic/molecular wave function mixings, the transition dipole moments of the $3^1\Delta_g$ and $4^1\Delta_g$ states strongly vary with internuclear distance, which suggests that the Franck−Condon Factors approximation will be inaccurate. In this article, detailed analyses, results, and discussions of the $3^1\Delta_g$ and $4^1\Delta_g$ states are presented for clearer illustration of the interaction picture between these twin states. This work focuses on new aspects of the detailed analysis of the previously observed $3^1\Delta_g$ and $4^1\Delta_g$ states. To see the behavior of curves' avoided crossing, values of $\Delta G_{v+1/2}$ and $B(v)$ calculated from either diabatic or adiabatic curves using Magnier's ab initio potentials are compared with our experimental data. Molecular constants (listed in tables) were derived from Dunham fits, and the RKR potentials were constructed for both the $3^1\Delta_g$ and $4^1\Delta_g$ states observed previously. Further, Λ-doubling splittings were estimated and characterized, (f-d) *l*-mixing between these twin states was discussed, and core-penetrating and core-nonpenetrating characters were addressed in this connection.

2. Experimental Setup

The details of the optical−optical double resonance (OODR) experimental setup with a block diagram can be found elsewhere.[13] The OODR technique is based on the simultaneous

* To whom correspondence should be addressed. Fax: 886-6-2747995. E-mail: chintsai@mail.ncku.edu.tw.
[†] Department of Chemistry.
[‡] Department of Physics.

10.1021/jp805479t CCC: $40.75
Published on Web 03/30/2009

interaction between a molecule (or an atom) and two photons that are in resonance with two molecular (atomic) transitions involving certain energy levels. In brief, the sodium vapor is produced in a five-arm stainless steel heat pipe oven maintained at a 350 °C stabilized temperature around its center using the combination of ceramic-isolated heaters and variacs and a pressure of about 1 Torr of argon buffer gas. An Ar^+ laser (Coherent I-90, total of nine lines; see Table 1 of ref 12) is used as a pump laser to populate the $B^1\Pi_u$ state from the thermally populated ground state $X^1\Sigma_g^+$ of the Na_2 system. The Ar^+ laser is intensity-modulated at 1 kHz and counterpropagated to the single-mode probe laser. Since the $B^1\Pi_u \rightarrow X^1\Sigma_g^+$ rovibrational transitions have been intensively studied by Kusch and Hessel,[15] we calculate the term values of the populated $B^1\Pi_u$ levels from their Dunham coefficients (set III in Table 7 in ref 15) instead of adding the ground-state term value to the laser frequency. A list of $B^1\Pi_u \rightarrow X^1\Sigma_g^+$ transitions is reported by Camacho et al.[16] A tunable cw ring-dye laser (Coherent 899-29 autoscan) pumped by a diode-pumped solid-state laser (Coherent Verdi-10) is used to probe the high-lying Rydberg states from the populated intermediate levels of the $B^1\Pi_u$ state.

The laser gain media Ti:sapphire crystal (lasing range of 12 800−14 400 cm^{-1}) and DCM (4-dicyanomethylene-2-methyl-6-*p*-dimethylaminostyryl-4H-pyran) dye (lasing range 14 300−16 500 cm^{-1}) are used in the cw ring laser to achieve the required probe laser frequency range. The laser power typically is about 500 mW at the center of gain medium and 100 mW on the edge. When the levels at the high-lying Rydberg states are probed, they undergo collisional energy transfer to populate the adjacent triplet gerade states.[17] Subsequently, UV fluorescence from these triplet gerade states to the $a^3\Sigma_u^+$ state (dissociates to the (3s + 3s) atomic limit) can be detected using a filtered photomultiplier tube (PMT) (filter: Sequoia-Turner Corp. 330−385 nm, photomultiplier tube: RCA84-22). The signals from the PMT are amplified by a lock-in amplifier (Stanford Research System SR-830) with the reference frequency of about 1 kHz by chopping the Ar^+ laser beam.

For the process of the data accumulation, the signals of UV fluorescence from the PMT, the I_2 excitation spectrum, and one of the etalon transmission fringes from the built-in wavemeter are simultaneously recorded and displayed on a personal computer. Recording of the etalon transmission fringes is for frequency continuity checking. The line positions of the OODR spectrum can be determined to within 0.02 cm^{-1}. The uncertainties are mainly from the near-sub-Doppler pumping of the thermally populated ground-state molecules by the frequency-fixed Ar^+ laser lines, from the laser power broadening, and from the collisional broadening. These uncertainties may include a shift of the line position up to ~0.2 cm^{-1} for the observed levels in the present work. Since the laser beams are counterpropagating, a major fraction of the Doppler shifts cancel. Thus, the total maximum experimental uncertainty in measuring the OODR line positions (including the sub-Doppler broadening, power broadening, and collisional broadening uncertainties) of the probed excited state can be 0.22 cm^{-1}.

3. Results and Analysis

3.1. Electronic State Assignments and Estimation of Λ-Doubling Constants. We have recorded nine sets of OODR spectroscopic data, including the intensities and wavenumbers of the excitation fluorescence signals for the processes ($^1\Sigma_g^+$, $^1\Pi_g$, $^1\Delta_g \leftarrow B^1\Pi_u \leftarrow X^1\Sigma_g^+$) corresponding to nine single-line Ar^+ pump laser lines. According to the selection rules of $\Delta\Lambda = 0, \pm1$, $\Delta S = 0$, and g ↔ u, the transitions from a $^1\Pi_u$ state to the $^1\Sigma_g^+$, $^1\Pi_g$, and $^1\Delta_g$ states are allowed, where Λ and *S* are the modulus of the projection of the total orbital angular momentum (*L*) on the internuclear axis and the total spin quantum number of the diatomic system Na_2, respectively. Since Λ can have the projection on either side of the center of the internuclear axis, the state with $\Lambda \neq 0$ splits into two components, the e-parity level and the f-parity level for each *J*, and the interaction between the nuclear rotational motion and the electronic orbital motion is responsible for this splitting, the so-called "Λ-doubling".[18] The detailed studies of Kusch et al.[15] and Camacho et al.[16] provided extensive information about the transitions from $X^1\Sigma_g^+$ to $B^1\Pi_u$. From our OODR recorded spectra, several obvious vibrational progressions of the patterns consisting of strong P, Q, and R lines have been identified (Supporting Information).

The procedure of tentative (v,*J*) assignments and the outline of the data analysis have been illustrated in ref 14. Figure 1 displays a part of the raw fluorescence spectrum of the vibrational progressions of the probed $^1\Delta_g(v,J)$ states excited from the intermediate rovibrational $B^1\Pi_u(v',J')$ state pumped by a single-line 496.5 nm Ar^+ laser. This sample spectrum clearly represents the closeness of the vibrational progressions belonging to two different $^1\Delta_g$ states excited from the same and different rovibrational $B^1\Pi_u(v',J')$ states in Na_2, for instance, $^1\Delta_g(v = 6,7;\ J = 42-44) \leftarrow B^1\Pi_u(7,43)$ and $^1\Delta_g(v = 3,4;\ J = 29-31) \leftarrow B^1\Pi_u(4,30)$; $^1\Delta_g(v = 6,7;\ J = 27-29) \leftarrow B^1\Pi_u(8,28)$. This shows that there are two sets of progressions very close to each other (v_3 being closest to $v_4 - 1$, where v_3 and v_4 stand for the vibrational quantum numbers of the 3 and $4^1\Delta_g$ states) in the energy range from 35 300 to 36 000 cm^{-1} (within one vibrational progression of about 100 cm^{-1}). For instance, the term values of the PQR lines for the transition excited from $B^1\Pi_u(10,12)$ to $J = J',J' \pm 1 = 11, 12, 13$, that is, at $[J(J + 1) - \Lambda^2] = 128$, 152, and 178, the vibrational progressions of $v_3 = 8-10$ and $v_4 = 7-9$ are very close to each other, and the separation increases gradually as progression goes higher. This feature has led to separate out the whole progression into two sets belonging to the $3^1\Delta_g$ and $4^1\Delta_g$ states. Calculations by Magnier et al.[1] show that for the 3 and $4^1\Delta_g$ states the v-spacings are ~100−120 cm^{-1} and the potential minima T_e of the $3^1\Delta_g$ and the $4^1\Delta_g$ states are separated by ~120 cm^{-1}, which makes vibrational ladders of the two states tending to overlap for $v_3 + 1 = v_4$ (Figure 2 in ref 14). Since transition dipole moments of the $3^1\Delta_g$ and $4^1\Delta_g$ states vary strongly with internuclear distance due to the avoided crossing, the simple Franck−Condon calculations (which assume a constant transition dipole moment at all *R*) will be poor and are not suitable for the absolute vibrational quantum number assignment of these states. The observed rovibrational levels in the spectra for the transitions $B^1\Pi_u(v',J') + h\nu_{probe} \rightarrow (T_{v,j})$ $3,4^1\Delta_g(v,J)$ are listed (Supporting Information).

Reference 14 (Figure 1) shows the $2^1\Delta_g$, $3^1\Delta_g$, and $4^1\Delta_g$ states arising from the 3p + 3p ($2^1\Delta_g$), 3s + 4d ($3^1\Delta_g$), and 3s + 4f ($4^1\Delta_g$) asymptotes, respectively, calculated by Magnier et al.[1] Two clear avoided crossings occur at 8 Å (between the 2 and $3^1\Delta_g$ states) and at 4 Å (between the 3 and $4^1\Delta_g$ states). These avoided crossings exchange the characters of the molecular wave functions of the electronic states from one to another at R= 8.0 and 4.0 Å and give rise to mixed character of the wave functions of the involved states around the points of avoided crossings. The observed energy region of interest is lower than 37 500 cm^{-1}. Therefore, only the second avoided crossing at 4 Å is important in this work. To see the effect of the avoided crossing, we have constructed a pair of diabatic potential curves,[4,5]

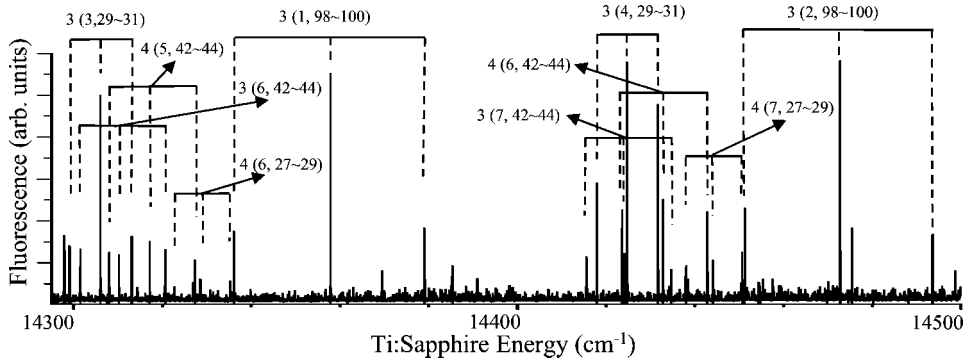

Figure 1. A typical part of the raw fluorescence spectrum of the vibrational progressions of the probed $^1\Delta_g(v,J)$ states excited from the same and different rovibrational intermediate $B^1\Pi_u(v',J')$ states pumped by a single-line 4965 nm Ar^+ laser to show the closeness of the vibrational progressions between two different electronic states ($3^1\Delta_g$ and $4^1\Delta_g$) of the same symmetry in Na_2. Identified progressions (v,J) belonging to the assigned $3^1\Delta_g$ and $4^1\Delta_g$ states are marked. The number (3 or 4) outside of the parentheses ($v,J' - 1$ to $J' + 1$) corresponds to the observed state ($3^1\Delta_g$ or $4^1\Delta_g$).

displayed in Figure 2, by removing four points near 4 Å, then exchanging the upper and lower points outside of the omitted points, and then spline-fitting the inner points and these outer points to form the 3 and $4^1\Delta_g$ diabatic potential curves, which include a crossing between them. The $3^1\Delta_g$ diabatic potential is the combination of the part of the $3^1\Delta_g$ for $R < 4$ Å and the part of the $4^1\Delta_g$ for $R > 4$ Å from Magnier's calculations. Likewise, the $4^1\Delta_g$ diabatic potential is the combination of the part of the $4^1\Delta_g$ for $R < 4$ Å and the part of the $3^1\Delta_g$ for $R > 4$ Å from Magnier's calculations. Now, we have the avoided crossing potentials (3, $4^1\Delta_g$ Magnier) from Magnier et al.,[1] ab initio calculations, and the approximate diabatic (deperturbed) crossing potentials (3,$4^1\Delta_g$ diabatic) of the 3 and $4^1\Delta_g$ states.

Figure 3 displays two sets of six $\Delta G_{v+1/2}$ versus $(v + 1/2)$ plots, three for the $3^1\Delta_g$ state and three for the $4^1\Delta_g$ states, derived from Magnier's adiabatic potentials (3,$4^1\Delta_g$ Magnier), the constructed diabatic potentials (3,$4^1\Delta_g$ diabatic), and the linear fitting of the experimentally observed data (3,$4^1\Delta_g$ expt). A comparison of these sets of $\Delta G_{v+1/2}$ versus $(v + 1/2)$ plots for the $3^1\Delta_g$ and $4^1\Delta_g$ states among Magnier's adiabatic potentials (3,$4^1\Delta_g$ Magnier), the constructed diabatic potentials (3,$4^1\Delta_g$ diabatic), and the linear fitting of the experimentally observed data (3,$4^1\Delta_g$ expt) shows that the variations of $\Delta G_{v+1/2}$ with $(v + 1/2)$ are smooth and linear for the diabatic states, while the $\Delta G_{v+1/2}$ values from Magnier and the experiment are different from the diabatic case. Though our observed values are not very similar to those of Magnier's calculations, the trends of the $\Delta G_{v+1/2}$ variations for both the $3^1\Delta_g$ expt and $4^1\Delta_g$ expt states are very similar to the corresponding trends of those variations for Magnier's adiabatic curves. Further, as seen from the two sets of the plots, the $\Delta G_{v+1/2}$ values of the $3^1\Delta_g$ Magnier and $3^1\Delta_g$ expt states are similar to those of the $3^1\Delta_g$ diabatic state in the range of $v < 4$, whereas the $\Delta G_{v+1/2}$ values of the $3^1\Delta_g$ Magnier and $3^1\Delta_g$ expt states are similar to those of the $4^1\Delta_g$ diabatic state for $v > 4$. Likewise, the $\Delta G_{v+1/2}$ values of the $4^1\Delta_g$ Magnier and $4^1\Delta_g$ expt states are similar to those of the $4^1\Delta_g$ diabatic state in the range of $v < 6$, whereas the $\Delta G_{v+1/2}$ values of the $4^1\Delta_g$ Magnier and $4^1\Delta_g$ expt states are similar to those of the $3^1\Delta_g$ diabatic state for $v > 6$. Figure 4 displays two sets of six $B(v)$ versus v plots, three for the $3^1\Delta_g$ state and three for the $4^1\Delta_g$ states, derived from Magnier's adiabatic potentials (3,$4^1\Delta_g$ Magnier), the constructed diabatic potentials (3,$4^1\Delta_g$ diabatic), and the linear fitting of the experimentally observed data (3,$4^1\Delta_g$ expt). Figure 4 illustrates similar types of trends in the two sets of six plots of the variations of $B(v)$ with v of the observed $3^1\Delta_g$ expt and $4^1\Delta_g$ expt states as in $\Delta G_{v+1/2}$ versus $(v + 1/2)$ plots, as well. In a word, in Figure 3, the trends of

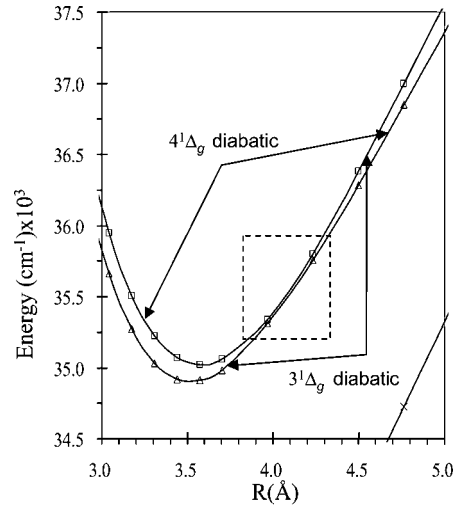

Figure 2. The plot of Magnier's calculations of the 3 and $4^1\Delta_g$ states; using these two potentials, we have constructed a pair of new diabatic potential curves by omitting the pairs of points at $R \sim 4.0$ and 4.2 Å for each state (shown in the inner box), then exchanging the upper and lower points outside of the omitted points, and then spline-fitting the inner points and these outer points to form the 3 and $4^1\Delta_g$ diabatic potential curves, which include a crossing between them. The curve at the lower right corner is a part of the $2^1\Delta_g$ state, which gives an idea of the separation between the $2^1\Delta_g$ state and the twin states, the 3 and $4^1\Delta_g$.

$\Delta G_{v+1/2}$ versus $(v + 1/2)$ and, in Figure 4, the trends of $B(v)$ versus v obtained from Magnier's calculations and the experimental values (individual linear fits) are very similar, but they are quite different from the trends of those obtained from the constructed diabatic potentials. Close agreements of the values of $\Delta G_{v+1/2}$ at different $(v + 1/2)$ in Figure 3 and the values of $B(v)$ at different v in Figure 4 between the linear fit of the observed data and Magnier's work suggest that all of the assignments to vibrational levels of the $3^1\Delta_g$ and $4^1\Delta_g$ states are correct and unambiguous. The above illustration indicates clearly the signature of the strong interactions between the observed twin $3^1\Delta_g$ and $4^1\Delta_g$ states in comparison to the constructed diabatic potentials of these states.

Previously, we reported the results of our observation of the $3^1\Delta_g$ and $4^1\Delta_g$ states from the individual linear fitting of the observed data fields.[14] In this method, we directly used G_v and B(v), which are the intercept and the slope of the linear fit (T_{vJ} versus $[J(J + 1) - 4]$) plot), respectively, to construct the RKR potentials ($3^1\Delta_g$ expt and $4^1\Delta_g$ expt), which exhibit a clear

avoided crossing at $R_c = 4.09$ Å and a splitting at $\Delta E_c = 75$ cm^{-1} between these two states, as depicted in ref 14. Magnier's calculations were plotted for a close comparison with the $3^1\Delta_g$ expt and $4^1\Delta_g$ expt states,[14] and it is quite clear that the lower curve of the twin states is the $3^1\Delta_g$ state and upper one is the $4^1\Delta_g$ state with the potential minima (T_e) of 34 757.07 and 34 886.81 cm^{-1}, respectively. The data fields[14] show the eigenvalues calculated from the constructed RKR potentials by the linear fits of the $3^1\Delta_g$ expt and $4^1\Delta_g$ expt states and the experimentally observed term values as a function of $[J(J + 1) - 4]$.

For a comparative study of the results from the linear fits,[14] to extract Λ-doubling effects involved in such strongly perturbed twin states (3 and $4^1\Delta_g$) and eventually to critically investigate the interactions between these two states, we have attempted to analyze the observed data in more detail using Dunham fits of the e-parity levels after separating out observed e/f-parity levels for both the $3^1\Delta_g$ and $4^1\Delta_g$ states. In order to determine the molecular constants and to estimate the discrepancy δ_{f-e}, which is the difference between the observed term value of the f-parity levels and the calculated term value from Dunham coefficients Y_{ij} of the e-parity levels of the same observed set of rovibrational quantum levels (v,J), we have performed the Dunham polynomial fit of the e-levels by the least-squares fitting to the eq 1 (Dunham double power series expansion) given below).

$$T_{v,J} = \sum_{i,j} Y_{ij}\left(v + \frac{1}{2}\right)^i [J(J + 1) - \Lambda^2]^j \qquad (1)$$

Here, Y_{ij} are the Dunham coefficients, and $\Lambda = 2$ for Δ states. For the $3^1\Delta_g$ state the PQR lines at $v = 0$ are excluded in the Dunham fitting for their sudden abnormal decrease with respect to those at $v \geq 1$. The manifestation of the Λ-doubling is in the splitting into e/f parity levels. The ground-state $X^1\Sigma_g^+$ does not involve any Λ-doubling since $\Lambda = 0$ and the levels are all of e-parity. For the pumped intermediate state $B^1\Pi_u$, Λ-doubling was considered by Kusch et al.[15] and Camacho et al.,[16] and the term values of the intermediate levels are regenerated using the molecular constants in ref 15. Considering the electric dipole transition, the selection rules for allowed transitions are e ↔ e, f ↔ f for both the P and R branches ($\Delta J = \pm 1$), and e ↔ f for the Q branch ($\Delta J = 0$).[18] A schematic diagram of e/f-level transitions can be found be in Figure 2 of ref 12.

In the Dunham fits, we have chosen the preset value (a "parameter" for the preset value of δ_{f-e} of the Dunham fit program) of the discrepancy to be $\delta_{f-e} = 0.7$ cm^{-1}; it is about 3 times the fitting error bar from the test Dunham runs for both of the states. This selection of the preset δ_{f-e} value in the Dunham fitting for both of the states allows us to obtain consistent and reasonable standard deviations which should be nearly equal to the total experimental uncertainly. By Dunham fit, this ensures that we obtain an acceptable set of observed e-level data and that we extract the corresponding acceptable set of observed f-level data due to Λ-doubling splitting (<1 cm^{-1}). The setting/choice of the "preset value of δ_{f-e}" in the Dunham fit run, in turn, allows us to sort out a reasonable/acceptable data set which generates molecular constants and thereby eventually the RKR potential. In the Dunham fit output files (Supporting Information), if δ_{f-e} of any one line of a PQR set is over the preset value of 0.7 cm^{-1}, that PQR set is a "deviant PQR set" and the rest are the 'nondeviant PQR set' in our Dunham fits. On the basis of this, 38 nondeviant e-levels and 30 f-levels in the range of $1 \leq v \leq 10$ and $11 \leq J \leq 44$ for the $3^1\Delta_g$ state and 142 nondeviant e-levels and 141 f-levels in the range of $3 \leq v \leq 25$ and $11 \leq J \leq 65$ for the $4^1\Delta_g$ state were found in the Dunham fit.

TABLE 1: The Molecular Constants (cm^{-1}) for the Present Experimental Results (Dunham Fit of the e-Parity Levels and Linear Fit) and for Magnier's Ab Initio Calculation[1] for the $3^1\Delta_g$ State of Na_2[a]

Y_{ij}	Dunham Fit of the e-parity levels	linear fit[14]	Magnier[1]
T_e	0.3475627×10^5 (0.3×10^1)	0.3475707×10^5	0.34606×10^5
Y_{10}	0.118874×10^3 (0.2×10^1)	0.1214×10^3	0.1274×10^3
Y_{20}	0.77731×10^0 (0.5×10^0)		
Y_{30}	-0.15180×10^0 (0.4×10^{-1})		
Y_{40}	0.58408×10^{-2} (0.2×10^{-2})		
Y_{01}	0.11426×10^0 (0.1×10^{-2})	0.116×10^0	0.118×10^0
Y_{11}	0.81936×10^{-3} (0.8×10^{-3})		
Y_{21}	-0.2758×10^{-3} (0.1×10^{-3})		
Y_{31}	0.1585×10^{-4} (0.7×10^{-5})		
Y_{02}	-0.1925×10^{-6} (0.2×10^{-6})		
q_0	-0.366×10^{-3} (0.2×10^{-3})		
q_v	0.583×10^{-4} (0.2×10^{-4})		
μ	0.16×10^{-6} (0.1×10^{-6})		
σ	0.2×10^0		

[a] The seemingly superfluous digits are necessary to compensate for the effects of correlations between the constants; σ is the standard deviation of the Dunham fit with e-levels.

After sorting out the e/f-parity levels of the observed data, we have performed the 10 parameter Dunham fits of the e-levels and obtained the values of δ_{f-e} of the $3^1\Delta_g$ and $4^1\Delta_g$ states. The dependence of δ_{f-e} (the δ_{f-e} columns in the Dunham output (Supporting Information) on $(v + 1/2)$ and $[J(J + 1) - \Lambda^2]$ for the $3^1\Delta_g$ and $4^1\Delta_g$ states is pictorially depicted (Supporting Information) for a clearer and easier view. For the $3^1\Delta_g$ state, v dependence of δ_{f-e} is clear, but it includes large fluctuations, while the $[J(J + 1) - \Lambda^2]$ dependence clearly shows an increasing trend. For the $4^1\Delta_g$ state, the v dependence of δ_{f-e} goes on increasing until $v = 12$ and then suddenly drops to around $\delta_{f-e} = 0$, but $[J(J + 1) - \Lambda^2]$ increases until about $J = 50$, and then, it seems to be steady. Since the energy of an f-level is lower than that of an e-level, we have attempted to estimate the Λ-doubling splitting constants (q_0, q_v, μ), taking only the f-levels corresponding to the negative values of δ_{f-e} in the Dunham fits for both the $3^1\Delta_g$ (19 f-levels) and the $4^1\Delta_g$ (91 f-levels) states. The estimated average value (standard deviation) of δ_{f-e} for the $3^1\Delta_g$ state is -0.37 cm^{-1} (0.31 cm^{-1}), and that for the $4^1\Delta_g$ state is -0.28 cm^{-1} (0.30 cm^{-1}). The three-parameter Dunham fit program was run using only all of the negative δ_{f-e} values obtained from the 10 parameter Dunham fit to derive three Dunham coefficients, which are the Λ-splitting constants (q_0, q_v, and μ). They are related to the Λ-doubling energy term ($T_{\lambda d}$) involving v and J through the modified Dunham expression as follows (eq 2).

$$T_{v,J} = \sum_{i,j} Y_{ij}\left(v + \frac{1}{2}\right)^i [J(J + 1) - \Lambda^2]^j + \delta[J(J + 1) - \Lambda^2] \times \left\{q_0 + q_v\left(v + \frac{1}{2}\right) + \mu[J(J + 1) - \Lambda^2]\right\} \qquad (2)$$

Here, the whole term multiplied by δ is $T_{\lambda d}$. In the above eq 2, $\delta = 0$ for e-parity levels, and $\delta = -1$ for f-parity levels. Tables 1 and 2 list the derived values of the molecular constants of the 3 and $4^1\Delta_g$ states, respectively. The molecular constants from Dunham fits are compared with those obtained from the linear fit[14] and Magnier's calculations[1] in Tables 1 and 2. The 10

TABLE 2: The Molecular Constants (cm^{-1}) for the Present Experimental Results (Dunham Fit of the e-Parity Levels and Linear Fit) and for Magnier's Ab Initio Calculation[1] for the $4^1\Delta_g$ State of Na_2[a]

Y_{ij}	Dunham fit of the e-parity levels	linear fit[14]	Magnier[1]
T_e	0.3488771×10^5 (0.8×10^0)	0.3488681×10^5	0.34726×10^5
Y_{10}	0.119080×10^3 (0.2×10^0)	0.1203×10^3	0.1218×10^3
Y_{20}	-0.11673×10^0 (0.2×10^{-1})		
Y_{30}	-0.11897×10^{-1} (0.1×10^{-2})		
Y_{40}	0.16352×10^{-3} (0.1×10^{-4})		
Y_{01}	0.11459×10^0 (0.4×10^{-3})	0.114×10^0	0.114×10^0
Y_{11}	-0.27389×10^{-3} (0.1×10^{-3})		
Y_{21}	-0.2150×10^{-4} (0.7×10^{-5})		
Y_{31}	0.4349×10^{-6} (0.2×10^{-6})		
Y_{02}	-0.3942×10^{-6} (0.1×10^{-7})		
q_0	0.346×10^{-3} (0.5×10^{-4})		
q_v	-0.935×10^{-5} (0.4×10^{-5})		
μ	-0.21×10^{-7} (0.2×10^{-7})		
σ	0.2×10^0		

[a] The seemingly superfluous digits are necessary to compensate for the effects of correlations between the constants; σ is the standard deviation of the Dunham fit with e-levels.

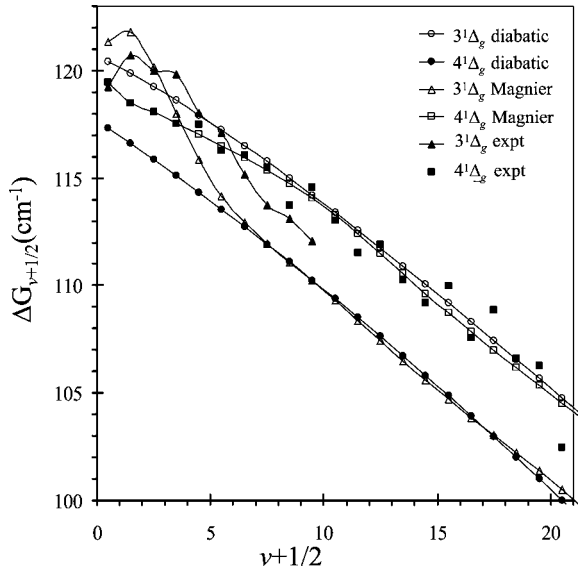

Figure 3. Two sets of six $\Delta G_{v+1/2}$ versus $(v + 1/2)$ plots, three for the $3^1\Delta_g$ state and three for the $4^1\Delta_g$ state, resulting from eigenvalue calculations using Magnier's adiabatic potentials ($3^1\Delta_g$ Magnier and $4^1\Delta_g$ Magnier), the constructed diabatic potentials ($3^1\Delta_g$ diabatic and $4^1\Delta_g$ diabatic), and the constructed RKR potentials ($3^1\Delta_g$ expt and $4^1\Delta_g$ expt) by linear fit of the experimentally observed data. See the text for detailed description and analysis.

parameter Dunham-fitted molecular constants were used to construct the RKR potential curves for the 3 and $4^1\Delta_g$ states of Na_2, which show an avoided crossing at $R_c = 4.10$ Å, displayed in Figure 5. Magnier's calculations are plotted for a close comparison with the observed $3^1\Delta_g$ expt and $4^1\Delta_g$ expt. Although the inner part of the $3^1\Delta_g$ expt state disagrees slightly with the $3^1\Delta_g$ Magnier state, the outer part of the $3^1\Delta_g$ expt agrees very well with the ab initio calculations.[1] The $4^1\Delta_g$ expt state is in excellent accord with the $4^1\Delta_g$ Magnier state. A detailed discussion of these two states is as follows.

3.2. The $3^1\Delta_g$ and $4^1\Delta_g$ States. We have assigned a total of 71 (40 e-levels and 31 f-levels) rovibrational levels in the range of $0 \le v \le 10$ and $11 \le J \le 44$ to the $3^1\Delta_g$ state and a total of 264 (142 e-levels and 122 f-levels) rovibrational levels in the range of $3 \le v \le 25$ and $11 \le J \le 65$ to the $4^1\Delta_g$ state. We have reported previously the observation of the $3^1\Delta_g$ and $4^1\Delta_g$ states,[14] but $v > 10$ levels of the $3^1\Delta_g$ state and $v = 0-2$ levels of the $4^1\Delta_g$ state are still unobserved. In addition to our previous attempt to construct the RKR potentials of the $3^1\Delta_g$ and $4^1\Delta_g$ states[14] from the intersect (G_v) and the slope ($B(v)$) of the linearly extrapolated observed vibrational progressions, in this work, we have constructed the RKR potentials of these two states (Figure 5) using the molecular constants derived from the Dunham fits of the observed e-parity rovibrational levels (excluding the PQR levels at $v = 0$ of the $3^1\Delta_g$ state for their abnormal values). Due to the presence of an avoided crossing, the constructed perturbed RKR potentials would not be accurate potentials. The vibrational eigenstates of neither the diabatic nor the adiabatic potential curves exactly represent the observed levels.[19] The difference arises between the (ΔG_v) and (B(v)) values obtained from exact adiabatic potentials and the observed values due to the neglect of the nonadiabatic terms in the resolution in the Schrodinger equation Hamiltonian. In order to reproduce the observed levels, we need to add the interaction matrix elements between the zero-order levels of the states taking either the $3^1\Delta_g$ diabatic$-4^1\Delta_g$ diabatic pair or the $3^1\Delta_g$ Magnier$-4^1\Delta_g$ Magnier pair. We have not found $v > 10$ for the $3^1\Delta_g$ state and $v < 3$ for the $4^1\Delta_g$ state, which restricts us within the range of $v_4 = 3-10$ for the relation $v_3 + 1 = v_4$. Therefore, in this study, we did not attempt to calculate the deperturbation energies of the vibrational levels of the $3^1\Delta_g-4^1\Delta_g$ pair of states to obtain a model of a pair of deperturbed potentials and an interaction matrix element. The important molecular properties of the $3^1\Delta_g$ state obtained from the Dunham polynomial fit are compared with our linear fit results and calculated values by Magnier et al.[1] in Table 1. The Dunham-fitted T_e, ω_e, and B_e values are very close to those of the linear fitted value, and they also agree well with the calculations.[1] The important molecular constants of the $4^1\Delta_g$ state derived from two different methods are compared with Magnier's calculations[1] in Table 2. The values of T_e, ω_e, and B_e are all in very good agreement. Displayed in Figure 5, the RKR potential constructed from Dunham coefficients of the $3^1\Delta_g$ state agrees very well with the ab initio calculated potential by Magnier et al.[1] (with very little lateral deviation). Similarly, the RKR potential constructed from Dunham coefficients of the $4^1\Delta_g$ state is in excellent agreement with the ab initio calculated potential.[1] The avoided crossing (R_c) and the energy splitting (ΔE_c) between the $3^1\Delta_g$ expt and $4^1\Delta_g$ expt states were found to be 4.09 Å and 75 cm^{-1}, respectively, by an individual linear fit method (Supporting Information), while those were found to be 4.10 Å and 94 cm^{-1}, respectively, by Dunham fit of the separated e/f-parity levels (Figure 5). The values of R_c derived from these two different methods are almost the same, but the value of ΔE_c is larger by 19 cm^{-1} when obtained from the Dunham fit method than that from the linear fit method. The Λ-doubling splitting constants (q_0, q_v, and μ) estimated from all of the negative values of δ_{f-e} in the Dunham fits of the 3 and $4^1\Delta_g$ states are also listed in the Tables 1 and 2, respectively, and will be discussed in the next section.

4. Discussion

In Figure 5, the RKR potential curves of the $3^1\Delta_g$ and $4^1\Delta_g$ states are found very close together as twin potentials. Their relative energy difference $\Delta E(4^1\Delta_g$ expt$-3^1\Delta_g$ expt) suggests that their is an avoided crossing at around 35 500 cm^{-1} (with a splitting of $\Delta E_c = 94$ cm^{-1}) at $R_c = 4.10$ Å. The crossing avoidance is applied with ab initio calculation; therefore, in a low-order approximation, the potential curves of these two states may intersect. In Magnier's calculations, the $3^1\Delta_g$ and $4^1\Delta_g$ states dissociate to 3s + 4d and 3s + 4f, respectively. According

to the noncrossing rule by Neumann and Wigner,[20] "for an infinitely slow change of internuclear distance, two electronic states of the same symmetry cannot cross each other", that is, the avoided crossing would be a point of crossing in a low-order approximation. As is evident from Figure 5, the interaction between the potential curves generates the avoided crossing at 4.10 Å between the twin almost parallel potential curves with very close potential minima ($\Delta T_e = 131.44\ cm^{-1}$). At R_c, the mutual interaction of these two states readily involves a mixing of two pure electronic states (i.e., configuration interaction of molecular wave functions) and a change over from one state to another state within a time interval of ($h/\Delta E$), where $\Delta E(4^1\Delta_g$ expt$-3^1\Delta_g$ expt$) = 94.0\ cm^{-1}$ in Figure 5 is the energy of separation due to the perturbation. This time interval is estimated to be $\Delta t = 0.35$ ps, which is nearly equal to the time period of the vibrational oscillation $h/\Delta G \sim 0.3$ ps, where ΔG is the successive separation of the vibrational levels. For these twin states of Na_2, the vibrational motion of the nuclei is not due to the average field produced by the electrons at different internuclear distances around R_c, but rather, the electronic and nuclear motions are coupled to each other, and the perturbation effect comes into play, giving rise to avoided crossing. If $\Delta E \gg \Delta G$, the switching over from one state to another occurs rapidly compared to the vibrational time period, whereas if $\Delta E \ll \Delta G$, the switching will happen only after a large number of oscillations; here, however, ΔE and ΔG are comparable ($\Delta E \approx \Delta G$).

As illustrated in the previous section, the effect of the avoided crossing is also reflected on the vibrational levels of the $3^1\Delta_g$ and $4^1\Delta_g$ states as a prominent disturbance in the $\Delta G_{v+1/2}$ versus $(v + 1/2)$ variations. This exhibits a substantial deviation from the linearity with unequal and irregular spacings of $\Delta G_{v+1/2}$ with $(v + 1/2)$ when $v \leq 9$. The nonlinear and irregular pattern is also clear in the $B(v)$ variation with v, which explains the mutual perturbation due to the avoided crossing. In addition, comparisons of the observed normalized intensities with the calculated Franck−Condon Factors between the $4^1\Delta_g$ and $B^1\Pi_u$ states taking $v^* = 2$, 3, and 4 (v^* is the tentative assignment of the vibrational energy level (v) because we did not observe the lowest vibrational energy level $v = 0$) for the lowest vibrational level of the $4^1\Delta_g$ state show that $v^* = 2$ could also be an acceptable assignment of the lowest vibrational level observed for the $4^1\Delta_g$ state (Supporting Information). This indicates that the perturbation has affected the vibrational levels near the avoided crossing region to push down the vibrational progressions of the $4^1\Delta_g$ state by one unit.

Though Λ-doubling splittings are quite clear from the δ_{f-e} values for both the 3 and $4^1\Delta_g$ states, the variations of δ_{f-e} as a function of $(v + 1/2)$ and $[J(J + 1) - 4]$ (Supporting Information) do not show any kind of clear smooth dependence; rather, fluctuations appear over the observed (v,J) ranges, and they also include positive values of δ_{f-e} for some v,J values. Considering the ranges $v < 12$ and $[J(J + 1) - 4] \sim 2000$, the Λ-doubling feature, that is, the dependence of δ_{f-e} on $(v + 1/2)$ and $[J(J + 1) - 4]$, is much clearer in the $4^1\Delta_g$ state compared to that in the $3^1\Delta_g$ state. For eq 2, the significant contribution of q_0 depends only on $[J(J + 1) - \Lambda^2]$, whereas that of q_v comes from both $[J(J + 1) - \Lambda^2]$ and $(v + 1/2)$, and that of μ depends on the square of $[J(J + 1) - \Lambda^2]$. Tables 1 and 2 list the derived values of these constants q_0, q_v, and μ, which are reasonable in view of their orders of magnitudes and are statistically meaningful. As seen from Tables 1 and 2, the values of the splitting constants q_0, q_v, and μ are opposite in sign in these two states. In the systems, like Na_2 having an even number of electrons, the Λ-doubling splitting eventually occurs due to the heterogeneous perturbations by a state of $\Omega = 0^+$ or 0^- symmetry, and this impacts the e- and f-levels in different ways. Figure 5 shows that the observed $4^1\Delta_g$ state matches quite nice with the Magnier's ab initio calculation, while the $3^1\Delta_g$ state deviates laterally from the ab initio calculation. The observed range of the vibrational levels of the $4^1\Delta_g$ state ($3 \leq v \leq 25$) is much wider than that of the $3^1\Delta_g$ state ($0 \leq v \leq 10$). It seems that the mutual strong perturbations between the twin states affected the heterogeneous perturbations caused by $\Omega = 0^+$ or 0^- symmetry, giving rise to the signature of the Λ-doubling splitting in each state. Therefore, the variations of δ_{f-e} on $(v + 1/2)$ and $[J(J + 1) - 4]$ do not show any kind of clear smooth trend with low fluctuation (Supporting Information) in Na_2. From the patterns of the $T_{v,J}$ levels illustrated in ref 14, revealing almost constant energy shifts as a function of $J(J + 1)$ between v_4 and $v_3 + 1$, one may expect the interactions to vary smoothly with J, if not with v. Similar problems arise in other alkali dimers, arising from spin−orbit interactions, for example, the D state in NaK, as described by Tamanis et al.,[21] where some q factors were simply tabulated as $q(v,J)$ experimentally but were retrieved after spin−orbit deperturbation. Probably, effects of multiple local perturbations and the inadequacy of the simple model of the Dunham expression used in this work are the reasons for no clear smooth trend of Λ-doubling in these twin states.

In the present case of Na_2, the perturbation arising from the kinetic energy of the Na nuclei is responsible for the noncrossing potential curves representation (adiabatic picture). The transition from the intermediate $B^1\Pi_u$ (3s + 3p) to the Na_2(3s + 4f) state by a single photon is asymptotically forbidden because $\Delta l = 2$, and thus, the Na_2 states correlating to (3s + 4f) may be difficult to observe in this experiment. Around the avoided crossing region, $E \sim E_c$, both the $3^1\Delta_g$ and $4^1\Delta_g$ can be observed as a mixture of two states. As the two nuclei speed up, they approach each other faster, the nuclear motion couples with the motion of the electrons, resulting in the Rydberg orbital shuffling and amplitude sharing among the molecular wave functions of the 3 and $4^1\Delta_g$ states, and a switch over from one state to another occurs due to the avoided crossing. In the united atom Rydberg orbital ($nl\lambda$, where the terms are usual) representation, the $3^1\Delta_g$(3s + 4d) state corresponds to the 4dλ state which splits into 4dσ, 4dπ, and 4dδ, and the $4^1\Delta_g$(3s + 4*f*) state corresponds to the 4fλ state, which forms 4fσ, 4fπ, 4fδ, and 4fφ. Due to the *l*-mixing, the interaction between *n*dσ and $(n + 1)$sσ is so strong that the two complexes are best described as a single supercomplex reported by Fredin et al.[22] for the NO-based molecule on the multichannel quantum defect theory (MQDT) which was developed by Jungen.[23] To our knowledge, no work has been reported on the combined OODR spectroscopy and MQDT study of the Na_2 system. However, the experiments on the NO system were carried out by OODR multiphoton ionization spectroscopy, and the data were analyzed using MQDT by Pratt et al.[24] and Gau et al.[25] The Rydberg states of NO were explained well in terms of (s−d)-mixing and (f−d)-mixing, giving rise to the supercomplexes for *n*s, *n*d, and *n*f Rydberg series. In the present case, our OODR data analyzed by a linear fit and the Dunham least-squares fit clearly show up two $^1\Delta_g$ states which appear as twin states with an avoided crossing. Owing to the studies and predictions of *l*-mixings in the NO system,[22−25] the present investigations of the Na_2 system can be explained as follows. These two observed 3 and $4^1\Delta_g$ states are perturbed, and the *l*-mixing occurs through the strong interaction around the avoided crossing region to form a supercomplex. Due to the transition from the intermediate $B^1\Pi_u$(3s + 3p) state by one

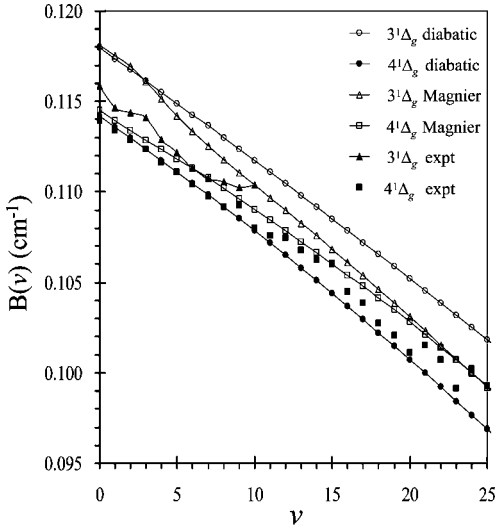

Figure 4. Two sets of six B(v) versus v plots, three for the $3^1\Delta_g$ state and three for the $4^1\Delta_g$ state, resulting from eigenvalue calculations using Magnier's adiabatic potentials ($3^1\Delta_g$ Magnier and $4^1\Delta_g$ Magnier), the adopted diabatic potentials ($3^1\Delta_g$ diabatic and $4^1\Delta_g$ diabatic), and the constructed RKR potentials ($3^1\Delta_g$ expt and $4^1\Delta_g$ expt) by linear fit of the experimentally observed data. See the text for detailed description and analysis.

photon, the $Na_2(3s + 4f)$ state is accessed by the (f−d)-mixing interactions occurring in the "4dδ−4fδ" orbital pair due to the molecular quadrupole moments leading to the formation of a single supercomplex which involves the properties of both the $3^1\Delta_g$ and $4^1\Delta_g$ states. This may also cause the lack of observation of the higher vibrational levels ($v > 10$) of the $3^1\Delta_g$ state. Some of the observed PQR lines are significantly perturbed as they show much larger δ_{f-e} values than the total maximum experimental uncertainty (0.22 cm^{-1}) of the PQR line positions. The appearance of such highly deviated line positions, most likely caused by the localized perturbations between 4d and 4f levels, could be attributed to the formation of nf-complexes in the Na_2 system. The intermediate $B^1\Pi_u$ state might have a very small amount of d-orbital character in the 3pπ orbital of Na_2. Overall, due to the transition from the intermediate $B^1\Pi_u(3s + 3p)$ state to the 3 and $4^1\Delta_g$ Rydberg states, the Na_2 system energy level structure changes from Hund's case (b) to Hund's case (d) due to the interactions of l-mixing. For higher Rydberg states, besides l-mixing between closely lying states, the phenomenon of l-uncoupling in the $5^1\Delta_g$ state of Na_2 was observed by Tsai and co-workers.[12] Very recently, from a detailed investigation on the rotational branch (PQR lines) intensity anomalies and position anomalies in the observed OODR spectra of the $n^1\Delta_g$ series ($n = 5-8$) of Na_2, Chaudhuri et al.[26] showed for the first time that, due to the effects of the L-uncoupling of the individual states and perturbations caused by the adjacent states, the same l-complexes (nd) approaching to the same ion core limits result in the same l-mixing processes which lead to the formation of the supercomplexes due to the anisotropy of the molecular ion $[Na_2^+(3s)]$ field in Na_2.

From a close examination of the sample spectrum displayed in Figure 1, it is clear that the intensities of the PR lines are about half of those of the Q lines, except for the ($v = 6,7$; $J = 42-44$) levels of the $3^1\Delta_g$ state, while the intensities of the PQR lines are comparable to one other in the $4^1\Delta_g$ state excited from the same intermediate rovibrational states and also from the different intermediate rovibrational states. According to the report by Pan et al.,[27] for the $^1\Delta_g \leftarrow {}^1\Pi_u$ transitions, the strong Q line should be accompanied by two half-intensity PR lines. These closely lying PQR levels of the v progressions of both of the $^1\Delta_g$ states are affected by the l-mixing interactions to share the amplitudes of the Rydberg orbitals, and hence, the irregular patterns in intensity in the spectra were observed. As seen from the intensity patterns in the spectrum (Figure 1), in contrast to the report by Pan et al.,[27] it seems that the Q line intensities of the $4^1\Delta_g$ state contribute to the Q line of the $3^1\Delta_g$ state, and PR lines intensities of the $3^1\Delta_g$ state contribute to the PR lines of the $4^1\Delta_g$ state. Thus, the intensity sharing among the rovibrationtal lines of the observed twin states is the direct reflection of the (f−d) l-mixing. From the $B^1\Pi_u(3s + 3p)$ state, by one-photon transition, the $4^1\Delta_g(3s + 4f)$ state has been observed due to the formation of 4f levels through (f−d) l-mixing involving the adjacent $3^1\Delta_g$ state. The l-mixings form a single supercomplex which consists of the molecular orbital properties of both of the twin states in Na_2. The adiabatic interaction between the twin $3^1\Delta_g$ and $4^1\Delta_g$ states strongly perturbed their molecular wave functions, causing mutual amplitude/intensity sharing, and resulted in the avoided crossing between these states.

Though we have observed energy levels $0 \le v \le 10$ of the $3^1\Delta_g$ state and $3 \le v \le 25$ of the $4^1\Delta_g$ state, the levels of $v > 10$ of the $3^1\Delta_g$ state and the levels of $v < 3$ of the $4^1\Delta_g$ state were not observed in this experiment. The lack of the observations of the levels of $v > 10$ of the $3^1\Delta_g$ state and the levels of $v = 0-2$ of the $4^1\Delta_g$ states is due to the strong interactions between these twin states through (f−d) l-mixing. It could be attributed to the fact that in the l-mixing, the contribution from "4d" to "4f" is larger than that from "4f" to "4d" when $R > R_c$, resulting in up to $v = 10$ for the $3^1\Delta_g$ state and up to $v = 25$ for the $4^1\Delta_g$ state in the present observation. Further, it could be attributed to the fact that in the l-mixing, the contribution from "4f" to "4d" is larger than that from "4d" to "4f" when $R < R_c$. The l-mixing interaction might pull/push down the vibrational levels near the bottom of the $4^1\Delta_g$ state, and the vibrational levels tend to pile up with the lower v- levels of the $3^1\Delta_g$ state. A process of diffusion/migration of the vibrational levels (lying below the avoided crossing) from the higher $4^1\Delta_g$ electronic state to the lower $3^1\Delta_g$ electronic state could be involved.

Further, according to the work by Li et al.,[9] on the basis of the core-penetrating and core-nonpenetrating states, almost all of the experimentally observed states belong to the category of the core-penetrating series, where $l < 3$. Since most of the Rydberg states of Na_2 were observed using a two-step excitation process via the intermediate states $A^1\Sigma_u^+$, $B^1\Pi_u$, and $b^3\Pi_u$, only low-l can be observed, guided by the propensity rule $\Delta l = \pm 1$. Considering the dominant hydrogenic $nl\lambda$ characters with the asymptotic limits, the core-penetrating $3^1\Delta_g(3s + 4d)$ was observed easily ($l = 2$ and $\Delta l = 1$ for 4d), while the core-nonpenetrating $4^1\Delta_g(3s + 4f)$ state was difficult to observe ($l = 3$ and $\Delta l = 2$ for 4f) before. This explains that it has been easy to observe the $3^1\Delta_g$ state right from $v = 0$ in this experiment. Notably, vibrational levels of the 3 and $4^1\Delta_g$ states nearest to the point R_c are the same $v = 4$, and the whole observed range of $v = 0-10$ of the outer turning points of the $3^1\Delta_g$ state spans $\sim R_c \pm 0.4$ Å. Thus, the avoided crossing at 4.10 Å and the twin appearance of the 3 and $4^1\Delta_g$ states establish the strong interaction and exchange of their individual pure properties around $R_c = 4.10$ Å. This enables us to observe $v = 3$ and 4 (partially) of the $4^1\Delta_g$ state with outer turning point $R_{v+} \approx R_c$ and several more vibrational levels with $R_{v+} > R_c$. It could be possible that due to the existence of strong interactions between these twin states, in the region of $R \ge R_c$, the $3^1\Delta_g$

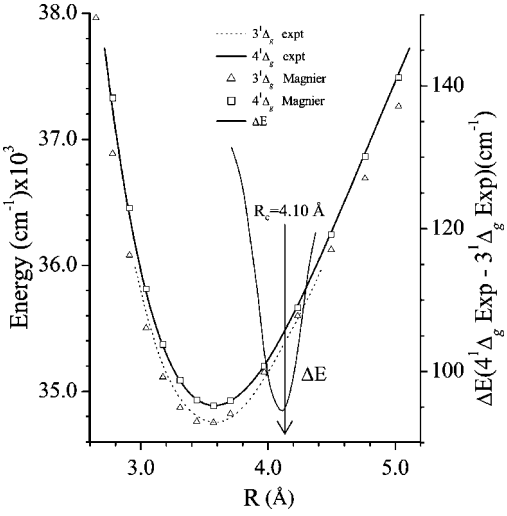

Figure 5. Constructed rotationless RKR potentials of the $3^1\Delta_g$ expt (dashed line) and $4^1\Delta_g$ expt (solid line) states versus internuclear distance R, using the derived molecular constants from the Dunham fits of the e-parity levels. Magnier et al. calculated (method B) values of the $3^1\Delta_g$ Magnier (open triangles) and $4^1\Delta_g$ Magnier (open squares) potential curves with their positions elevated by 150 and 160 cm^{-1}, respectively, for close comparison. The ordinate on the right-hand side is the energy difference [$\Delta E(4^1\Delta_g$ expt $- 3^1\Delta_g$ expt)] between the constructed RKR potentials of the $4^1\Delta_g$ expt and $3^1\Delta_g$ expt states. A clear avoided crossing around $R_c = 4.10$ Å and $\Delta E_c = 94$ cm^{-1} (very small compared to the potential depth of ~6000 cm^{-1}) is marked.

state looses its core-penetrating character and gains core-nonpenetrating character from $4^1\Delta_g$, and vice versa. Therefore, the levels $v > 10$ of the $3^1\Delta_g$ state were not observed; rather, more higher v levels of the $4^1\Delta_g$ state were observed. This implies that for the strongly coupled states of the same symmetry, particularly for twin states, it is difficult to interpret the possibility of experimental observations of the electronic state(s) on the basis of the core-penetrating and core-nonpenetrating categories. According to Li et al.,[9] in either case, the signals observed should belong to the penetrating (dδ) or (pp) state. However, on the contrary, the core-nonpenetrating $2^1\Delta_g$ state having an avoided crossing with the $3^1\Delta_g$ state at around $R = 8$ Å was observed using same experimental setup of OODR spectroscopy by Tsai and co-workers.[13]

5. Conclusions

In the present experimental observations of two singly excited Rydberg states, the $3^1\Delta_g$ and $4^1\Delta_g$, of Na_2 using cw optical−optical double resonance spectroscopy, the assignments of the absolute vibrational numbering of the two observed $^1\Delta_g$ states were accomplished by a comparison between the successive separations of the vibrational energy levels of Magnier's ab initio calculations and the linear fits of the observed energy levels. In order to critically investigate these twin states of Na_2, molecular constants were derived from the separated e/f-parity level Dunham fits, and they were found to compare very well with those obtained from the linear fit method of the observed energy levels and Magnier's calculations of both the $3^1\Delta_g$ and $4^1\Delta_g$ states. The constructed RKR potential curves from the derived Dunham coefficients of these states agree very well with Magnier's calculations. These two states are clumped together as twins with an avoided crossing at internuclear distance $R_c =$ 4.10 Å with $\Delta E_c = 94$ cm^{-1}. From the obvious features of the Λ-doubling splittings, we have estimated the splitting constants q_0, q_v, and μ for the 3 and $4^1\Delta_g$ states, but both states have failed to exhibit any particular low-fluctuation smooth dependence of the Λ-doubling splitting on the vibrational and rotational quantum numbers. The lack of smooth dependence or trend of Λ-doubling splitting on v and J quantum numbers is presumably due to multiple local perturbations in these twin states, apart from strong mutual perturbations between them, and the simple model of Dunham expression used in this work is not appropriate for these twin states of Na_2.

The one-photon transition from the intermediate $B^1\Pi_u(3s + 3p)$ state to the forbidden $Na_2(3s + 4f)$ state is explained in terms of the (f−d) l-mixing due to the molecular quadrupole moments, leading to the formation of a single supercomplex which involves the $nl\lambda$-molecular characters of the 3 and $4^1\Delta_g$ states. In Na_2, the adiabatic interaction between these perturbed twin states is so strong that the amplitude/intensity (molecular orbital characters) sharing occurs between these states, and eventually, an avoided crossing is formed between them. This work on the Na_2 system is an observation of "the noncrossing rule of the potential curves having the same symmetry". In the case of closely lying same-symmetry electronic states, the adiabatic interaction and exchange of the molecular wave function properties play an important role in making the characters of the vibrational levels of the involved states complicated. Vibrational levels near the bottom of a potential curve lying closely to the other electronic state (as a twin) could have a tendency of migration into the vibration levels belonging to the relatively lower electronic state in the region of $R < R_c$. Due to the wave function mixing among the 2, 3, and $4^1\Delta_g$ states having avoided crossing(s), the transition dipole moments between the intermediate $B^1\Pi_u$ state and any of these mixed states strongly depend on the internuclear distance and would really be interesting problems to investigate. This observation of avoided crossing due to the adiabatic mutual perturbation of molecular wavefunctions of the twin states in the Na_2 system would draw attention to investigate other alkali dimers and shed light on the interaction nature for better and clearer understanding.

Acknowledgment. We gratefully acknowledge the support of this work by the National Science Council, Taiwan.

Supporting Information Available: (1) The observed rovibrational levels of the $3^1\Delta_g$ and $4^1\Delta_g$ states of Na_2, (2) output of the Dunham fits of the e-parity levels of the $3^1\Delta_g$ and $4^1\Delta_g$ states of Na_2, (3) δ_{f-e} versus $(v + 1/2)$ and versus $[J(J + 1) - 4]$ plots of the $3^1\Delta_g$ and $4^1\Delta_g$ states of Na_2, and (4) comparison of the experimental normalized intensities and the Franck−Condon factors between the $B^1\Pi_u$ and $4^1\Delta_g$ states. This material is available free of charge via the Internet at http://pubs.acs.org.

References and Notes

(1) Magnier, S.; Milliè, Ph.; Dulieu, O.; Masnou, S. F. *J. Chem. Phys.* **1993**, *98*, 7113.
(2) Magnier, S. Ph. D. Thesis, Universite De Paris-Sud, Centre D'orsay, France, 1993.
(3) Knöckel, H.; Johr, T.; Richter, H.; Tiemann, E. *Chem. Phys.* **1991**, *152*, 399.
(4) Wang, H.; Whang, T. J.; Lyyra, A. M.; Li, L.; Stwalley, W. C. *J. Chem. Phys.* **1991**, *94*, 4756.
(5) Tsai, C. C.; Bahns, J. T.; Whang, T. J.; Wang, H.; Stwalley, W. C.; Lyyra, A. M. *Phys. Rev. Lett.* **1993**, *71*, 1152.
(6) Cooper, D. L.; Barrow, R. F.; Vergès, J.; Effantin, C.; D'Incan, J. *Can. J. Phys.* **1984**, *62*, 1543.
(7) Ratliff, L. P.; Wagshul, M. E.; Lett, P. D.; Rolston, S. L.; Phillips, W. D. *J. Chem. Phys.* **1994**, *101*, 2638.
(8) Tsai, C. C.; Bahns, J. T.; Stwalley, W. C. *J. Chem. Phys.* **1993**, *99*, 7417.

(9) Li, J.; Liu, Y.; Dai, X.; Li, L.; Field, R. W. *J. Chem. Phys.* **2001**, *114*, 7859.
(10) Barrow, R. F.; Amiot, C.; Vergès, J.; d'Incan, J.; Effantin, C.; Bernard, A. *Chem. Phys. Lett.* **1991**, *183*, 94.
(11) (a) Carlson, N. W.; Taylor, A. J.; Jones, K. M.; Schawlow, A. L. *Phys. Rev. A* **1981**, *24*, 822. (b) Carlson, N. W.; Taylor, A. J.; Schawlow, A. L. *Phys. Rev. Lett.* **1980**, *45*, 18.
(12) Chang, R. Y.; Whang, T. J.; Cheng, C. P.; Tsai, C. C. *J. Chem. Phys.* **2005**, *123*, 224303.
(13) Whang, T. J.; Wu, H. W.; Chang, R. Y.; Tsai, C. C. *J. Chem. Phys.* **2004**, *121*, 010513.
(14) Chen, W. X.; Chang, R. Y.; Whang, T. J.; Chaudhuri, C.; Tsai, C. C. *Chem. Phys. Lett.* **2007**, *439*, 29.
(15) Kusch, P.; Hessel, M. M. *J. Chem. Phys.* **1978**, *68*, 2591.
(16) Camacho, J. J.; Pardo, A.; Poyato, J. M. L. *J. Phys. B* **2005**, *38*, 1935.
(17) Li, L.; Field, R. W. *J. Mol. Spectrosc.* **1986**, *117*, 245.
(18) Herzberg, G. *Molecular Spectra and Molecular Structure I. Spectra of Diatomic Molecules*, 2nd ed.; Krieger Pub Co: Malabar, FL, 1989.
(19) Brion, H. L.; Field, R. W. *The Spectra and Dynamics of Diatomic Molecules*; Elsevier: Amsterdam, The Netherlands, 2004; Chapter 3, p 174.
(20) Neumann, J. V.; Wigner, E. *Phys. Z.* **1929**, *467*, 30.
(21) Tamanis, M.; Auzinsh, M.; Klincare, I.; Nikolayeva, O.; Ferber, R.; Pazyuk, E. A.; Stolyarov, A. V.; Zaitsevskii, A. *Phys. Rev. A* **1998**, *158*, 1932.
(22) Fredin, S.; Gauyacq, D.; Horani, M.; Jungen, Ch.; Lefevre, G.; Seeuws, F. M. *Mol. Phys.* **1987**, *60*, 825.
(23) Jungen, Ch. *J. Chem. Phys.* **1970**, *53*, 4168.
(24) Pratt, S. T.; Jungen, Ch.; Miescher, E. *J. Chem. Phys.* **1989**, *90*, 5971.
(25) Gauyacq, D.; Roche, A. L.; Seaver, M.; Colson, D. S.; Chupka, W. A. *Mol. Phys.* **1990**, *71*, 1311.
(26) Chaudhuri, C.; Chang, R. Y.; Tsai, C. C.; Cheng, C. P.; Whang, T. J. *J. Chem. Phys.* **2008**, *129*, 24303.
(27) Pan, Y. L.; Ma, L. S.; Ding, L. E.; Sun, D. P. *J. Mol. Spectrosc.* **1993**, *162*, 178.

JP805479T